Virtual Antenna Array with Directional Antennas for Millimeter-Wave Channel Characterization

Li, Mengting; Zhang, Fengchun; Ji, Yilin; Fan, Wei

Published in:
I E E E Transactions on Antennas and Propagation

DOI (link to publication from Publisher):
10.1109/TAP.2022.3161334

Publication date:
2022

Document Version
Accepted author manuscript, peer reviewed version

Virtual Antenna Array with Directional Antennas for Millimeter-Wave Channel Characterization

Mengting Li, Fengchun Zhang, Yilin Ji and Wei Fan

***Abstract*—Millimeter-wave (mm-Wave) band channel modeling and characterization are essential for system design and analysis in the fifth generation (5G) and future communication systems. Reliable channel sounding in the deployment scenarios is required for accurate and realistic channel modeling and characterization. In the state-of-the-art, directional scanning sounding (DSS) and virtual antenna array (VAA) sounding are two popular methods due to their simplicity and cost-effectiveness. The DSS and the VAA methods are typically based on mechanically rotatable directional antennas and mechanically movable omnidirectional antennas, respectively. However, the spatial resolution is limited by the directivity and high side lobes of the directional antennas used in the DSS method. The conventional VAA method also has limitations in terms of the low signal-to-noise ratio (SNR) and the unavailability of suitable omnidirectional antennas that support mmWave (above 60 GHz) band measurements and wideband horizontal polarization measurements. In this paper, a novel directional antenna based VAA framework in combination with the associated beamforming algorithm is proposed. Compared to the state-of-the-art methods, the proposed framework can achieve high angular resolution and high SNR for mm-Wave channel measurements without introducing additional cost and measurement time. Furthermore, it is a generic solution which can be applicable for arbitrary frequency bands and polarizations, unlike the conventional VAA method. To validate the effectiveness and robustness of the proposed method, experiments in two scenarios (a clean anechoic chamber and a realistic indoor meeting room) were conducted over 28 – 30 GHz with two types of directional antennas (i.e., a horn antenna and a corrugated antenna). Besides, the advantages of the proposed method are highlighted with a comparison to the conventional VAA and DSS methods.**

***Index Terms*—Beamforming, channel sounding, directional antennas, Millimeter-wave (mm-Wave), virtual antenna array.**

I. Introduction

MILLIMETER-wave (mm-Wave) and sub-Terahertz (THz) technologies have attracted considerable attention from both academia and industry due to their potential to meet the demands of high data rate in the fifth generation (5G) and future communication systems [1]–[4]. Accurate Channel characterizatoin in mm-Wave bands is of great importance for mm-Wave wireless technologies with respect to the communication system design and performance analysis [5]–[7]. Reliable and accurate channel sounding is crucial for channel modeling and characterization.

Numerical simulation tools [8]–[10] have been investigated by many research groups to explore the mm-Wave channels. However, the measurement-based methods are indispensible for characterizing the realistic scenarios which are much more complicated than the simulated scenarios. Many researchers have made efforts to investigate channel spatial profiles through measurements. Directional scanning with a single high directivity antenna, also called as directional scanning sounding (DSS) [11]–[13] is widely used in mm-Wave channel measurements. The DSS method is usually achieved by a horn antenna mechanically rotated on a turntable, which can capture the signals from different directions. However, the angular resolution is limited by the beam-width of the antenna and the side-lobe effects can also jeopardize the estimation results of multipath components (MPC)s [14]. Phased array based channel sounders [15]–[17], which measure the spatial channels using fast electronic beam-steering approach, have attracted much attention from academia due to its capability of measuring dynamic channels. However, this method typically suffers from high side-lobes and limited steering range. Switch arrays [18], [19], i.e., different physical antenna elements are connected via an electronic switch to a single RF chain can be an option to make a compromise between cost and measurement duration. Appropriate array processing technique is required to achieve high angular resolution for switch arrays. Antenna arrays with parallel radio frequency (RF) chains [20], [21], i.e., one RF chain for each antenna element can measure channels in high dynamic environments. However, both the switch arrays and antenna arrays with parallel RF chains need to deal with complicated calibration procedures in mm-Wave bands.

VAA is a popular and cost-effective method for measuring static mm-Wave channels [5], [22]–[25]. The basic idea is that a single omnidirectional antenna element can be moved to different spatial positions by a positioner forming arbitrary array configurations, such as uniform circular arrays (UCA) [22], [23], rectangular arrays [5] and uniform cubic arrays [24]. The limitations of current VAA method using omnidirectional antennas for mm-Wave band channel measurements are as follows: 1) Wideband omnidirectional antennas beyond 60 GHz are hard to be obatined commercially. 2) The horizontal polarized omnidirectional antenna operated in mm-Wave bands are much more difficult to design [26] and even unavailable commercially. This is a current bottleneck for validating channel polarimetric profiles for multiple-input-multiple-output (MIMO) over-the-air (OTA) studies in frequency range (FR2) [27], since both vertical and horizontal polarization measurements are required for channel polarimetric profile analysis [28]. 3) Omnidirectional antennas have low antenna gain which provides poor signal-to-noise ratio (SNR) and

Mengting Li, Fengchun Zhang, Yilin Ji and Wei Fan are with the Antenna Propagation and Millimeter-wave Systems (APMS) section, Aalborg University, Denmark.

Corresponding author: Wei Fan (Email: wfa@es.aau.dk).

constrains the measurement range, which is a major problem for high frequency bands.

Based on the previous discussions, a directional antenna based VAA framework is promising for mm-Wave and sub-THz channel characterization. This new framework can benefit from the use of both high gain antenna element and VAA scheme. Nevertheless, it becomes challenging to achieve a directional antenna based VAA in the following three aspects. The first issue lies on the beamforming procedure. To totally align the phase of each VAA element, the precise knowledge of antenna phase pattern is required [29]. However, the phase pattern is difficult to obtain in reality since it requires accurate complex antenna pattern measurement in an anechoic chamber and pre-knowledge of the antenna under test (AUT), e.g. phase center location. The effects of directional antenna phase pattern on the beamforming results are not investigated in the literature. Besides, we have found that in this work high back-lobe appears in the directional antenna based UCA beam pattern when using convetional classical beamforming (CBF) method for omnidirectional antenna based UCA as discussed in detail in Section II-C. Note that these are not problems for omnidirectional antennas since they usually have known, stable phase centers and flat phase pattern over broad angles. Moreover, since the investigations of directional antenna based VAA are missing in the literature, the requirement of the directional antenna used to form a VAA (i.e. which directional antenna is more suitable for VAA scheme) is an open question.

In this paper, we attempt to achieve VAA concept based on directional antennas for mm-Wave channel characterization. The proposed method can further improve the angular resolution and suppresses sidelobe effects compared to DSS method. It is worth noting that the benefits can be obtained without additional measurement time or cost since the measurement setup for VAA based on directional antenna and the DSS is essentially the same with the exception that the directional antenna is off-centered to form the UCA. We discussded and validated the proposed directional antenna based VAA scheme over 28-30 GHz. However, it can be used in all frequencies in principle. It has the potential of conducting polarization analysis and longer range measurements in sub-THz bands since dual-polarized high gain antennas operating in this band are commercially available. The main contributions of this paper are summarized as follows:

- The phase pattern and phase center stability of two different kinds of common directional antennas used for VAA scheme, i.e. a horn antenna and an open waveguide based corrugated antenna, are analyzed.
- A modified classical beamforming algorithm is proposed for directional antenna based UCA.
- Comparisons with the DSS and the convectional omni-directional antenna based VAA are provided in terms of angular resolution, delay resolution, and estimated path power.
- Comparisons with the performances of horn and corrugated antenna based VAA are provided and the selection of the diretional antenna element is discussed.
- Simulations, and experiments in the anechoic chamber and an indoor meeting room are conducted to validate the proposed framework.

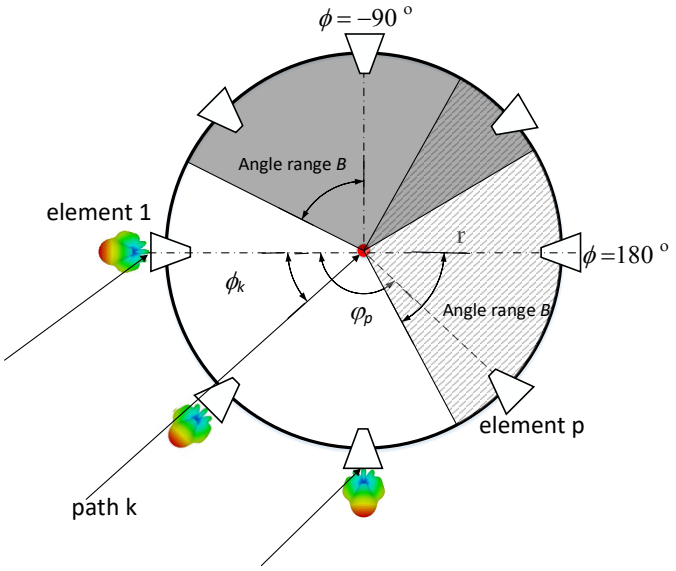

Fig. 1. An illustration of the UCA in a multipath channel.

The rest of this paper is structured as follows. Section II analyzes the phase pattern and phase center of three antennas used in this paper and proposes a modified CBF algorithm for directional antenna based VAA framework. Section III analyzes and compares the simulation results of conventional omnidirectional antenna based VAA, DSS method and the proposed method. Section IV validates the proposed method in an anechoic chamber and an indoor scenario. Comparisons with the conventional omnidirectional antenna based VAA and DSS methods are provided as well. Section V concludes the paper.

II. Method

A. Signal Model

In the following discussions, a UCA is taken as an example to illustrate the proposed concept since it can measure the multipaths from 0-360° in the azimuth plane with uniform beam pattern and can be easily compared with DSS method. Note that the proposed directional antenna based VAA framework is not limited to any specific array configuration. Assume a UCA composed of P directional antenna elements uniformly distributed on a circle with radius r as shown in Fig. 1. The angular position of the p-th element is $\varphi_p = 2\pi \cdot (p-1)/P, p \in [1, P]$. The spacing between two adjacent antenna elements should not be larger than $\lambda/2$ (λ is the free space wavelength of the working frequency) to avoid spatial aliasing effects [30]. Note that the signal model is a simplified 2-D model, i.e. all multipath components (MPCs) are confined to the azimuth plane. Assume that there are K multipath plane waves impinging on the UCA with the incident angle of ϕ_k. The frequency response at the UCA center can be expressed as

$$H(f) = \sum_{k=1}^{K} \alpha_k \exp(-j2\pi f \tau_k) \ , \tag{1}$$

where α_k and τ_k represent the complex amplitude and delay of the k-th path ($k \in [1, K]$), respectively. $f \in [f_L, f_U]$ is the frequency band of interest. The channel frequency response of the p-th array element is the superposition of the channel frequency responses of the K paths, which can be given by

$$H_p(f) = \sum_{k=1}^{K} \alpha_k \exp(-j2\pi f \tau_k) \ \cdot a_p(f, \phi_k), \tag{2}$$

where $a_p(f, \phi_k)$ is the array manifold coefficient of the p-th array element of the k-th path which can be expressed as

$$a_p(f, \phi_k) = \exp(\frac{j2\pi fr}{c} cos(\phi_k - \varphi_p)) g(f, \phi_k - \varphi_p), \tag{3}$$

where c is the speed of light. $g(f, \phi)$ is the complex radiation pattern of the antenna element.

The classical beamforming result can be obtained by

$$Q(f, \phi) = \sum_{p=1}^{P} \omega_p(f, \phi) \cdot H_p(f) \ , \tag{4}$$

where ω_p is the complex weight assigned to the p-th antenna element. The choice of ω_p is of great importance since it affects power angle profile performance of the VAA in terms of angular resolution and SNR. To align the phase of array elements and maximally combine their respective contributions [29], ω_p should be:

$$\omega_p(f, \phi) = \frac{a_p^*(f, \phi)}{\sum_{i=1}^{P} \mid a_i(f, \phi) \mid}, \tag{5}$$

where $(\cdot)^*$ represents the complex conjugate operator. The principle of this weight assignment is to completely align the phase of array elements considering both the phase pattern of antenna element and array configuration. However, the accurate phase pattern is generally not provided in the datasheet. The phase center locations of common directional antennas such as horn antennas or open-ended waveguide based antennas are usually unknown. To make directional antenna based UCA a practical method, it would be desirable that we can achieve the VAA scheme without a-prior knowledge of the complex antenna element pattern. Nevertheless, this issue can be neglected in omnidirectional antenna based UCA. Assuming an ideal omnidirectional antenna pattern, the array weights in (5) can be simplified as

$$\omega_p(f, \phi) = \frac{1}{P} \exp[-\frac{j2\pi fr}{c} cos(\phi - \varphi_p)]. \tag{6}$$

An ideal omnidirectional antenna has a stable phase center and the phase pattern is a constant for all angles in the azimuth plane. Thus, there is no need to consider the phase pattern. Moreover, the antenna gain can be easily removed since all the array elements receive the same signal power under the far-field condition. For directional antenna based VAA, it is necessary to analyze the phase pattern and phase center stability of the antenna element for designing array weights and achieving beamforming without knowing precise complex radiation pattern of antenna element. The discussions of the proposed modified CBF algorithm for directional antenna based UCA will be presented later in Section II-C.

TABLE I
ANTENNA SPECIFICATIONS

Antenna type	Frequency range (GHz)	HPBW (deg)	Gain[a] (dBi)
Biconical antenna	2-30	omnidirectional	6
Corrugated antenna	26.5-40	40	13.5
Horn	18-40	20	19

[a] Evaluated at 28-30 GHz.

TABLE II
MEASUREMENT SPECIFICATIONS

Parameter	Specifications
Frequency span & sweep points	28-30 GHz; 1001 points
Rotation range & step	-179°-180°; 1°
RF dynamic range	70 dB
Alignment	Laser tracker

Finally, the channel impulse response in the joint delay-angular domain can be calculated via inverse Fourier transformation:

$$h(\tau, \phi) = \sum_{f=f_L}^{f=f_U} Q(f, \phi) \cdot \exp(j2\pi f \tau) \ . \tag{7}$$

B. Phase Pattern and Phase Center Analysis

As discussed, it is essential to analyze the characteristics of phase pattern and phase center of directional antennas to propose a more practical array weighting scheme compared with (6) and analyze the potential error sources of the proposed method. A horn antenna [31] (model number: SAS-574) and a corrugated antenna [32] (model number: ASY-CWG-S-265) are used as examples to investigate their phase pattern and phase center stability, since they are representative in our analysis. A wideband biconical antenna [33] (model number: SZ-20030000/P) with omnidirectional radiation pattern in the azimuth plane is also analyzed for comparison purpose. The specifications of these antennas are shown in Table I according to the datasheets. The horn antenna is widely used in the DSS method and can be easily obtained in the RF laboratories. The corrugated antenna is a near-field probe antenna which is known to have quite stable phase pattern and phase center. In addition, these two antennas have different radiation performances in terms of half power beamwidth (HPBW), side lobes and phase pattern. These two directional antennas are intentionally selected to validate the robustness of the proposed method and investigate the requirements of the directional antennas used for forming a VAA in channel measurements.

We measured the complex radiation patterns of these antennas over 28-30 GHz in an anechoic chamber. Note that the antennas are carefully aligned with the rotation center in the measurements. The specifications of the complex antenna pattern measurements are summarized in Table II. Fig. 2 shows the normalized gain pattern of three antennas at 28, 29 and

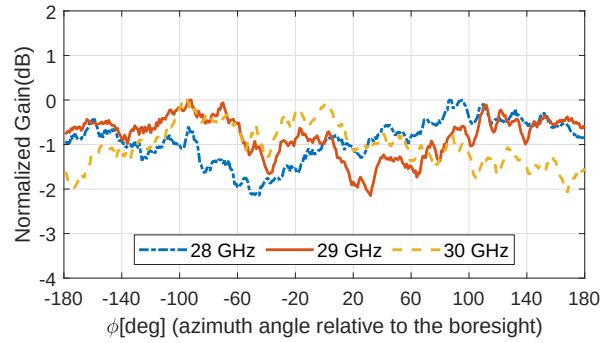

(a)

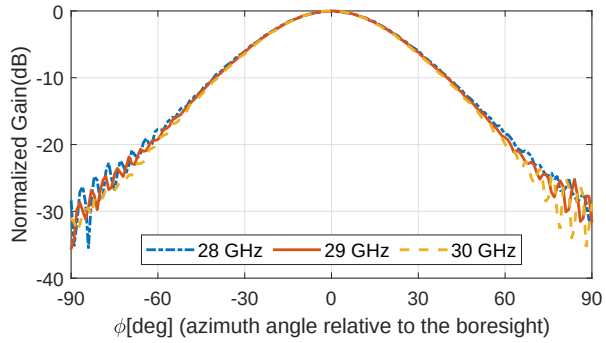

(b)

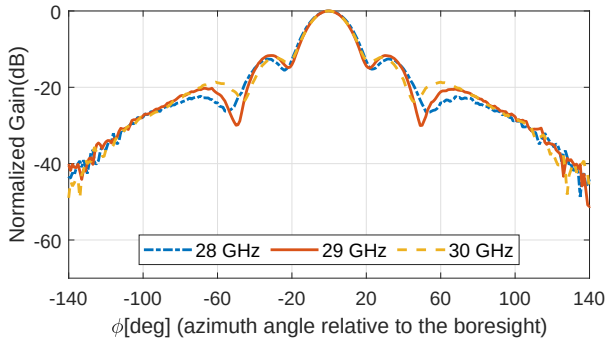

(c)

Fig. 2. Normalized gain patterns of (a) biconical antenna, (b) corrugated antenna, and (c) horn antenna at 28, 29 and 30 GHz.

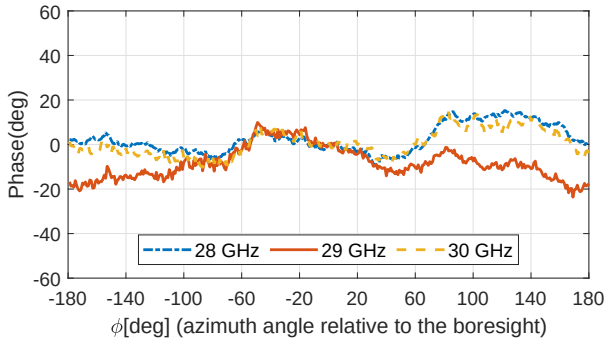

(a)

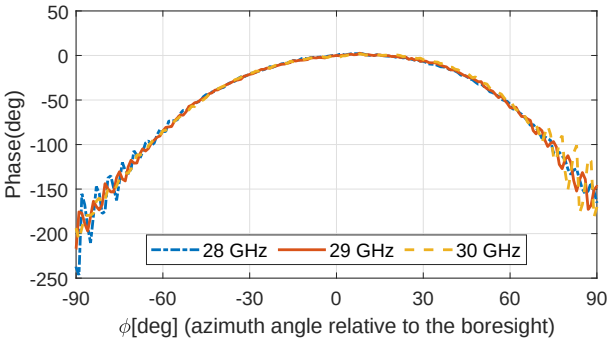

(b)

(c)

Fig. 3. Normalized phase patterns of (a) biconical antenna, (b) corrugated antenna, and (c) horn antenna at 28, 29 and 30 GHz.

30 GHz. For corrugated and horn antenna, only measured data within [-90°, 90°] and [-140°, 140°] are considered, respectively, due to the dynamic range in the measurements. The radiation pattern of biconical antenna is almost omnidirectional with up to 2 dB ripples. Fig. 3 depicts the normalized phase pattern of different antennas at 28, 29 and 30 GHz. The phase pattern fluctuation for biconical antenna at different frequency points is within 20° for all the angles. Corrugated antenna has almost the same phase pattern in different frequencies whithin [-90°, 90°] and the variation of the phase pattern is relatively small within [-40°, 40°]. Except for the angles around ±50°, horn antenna also has similar phase pattern for different frequencies and a flat phase pattern can be observed within [-20°, 20°].

The raw phase data Φ_{mea} measured in the anechoic chamber can be expressed as

$$\Phi_{mea}(f,\phi) = -\frac{2\pi f R}{c} + \psi(f,\phi), \tag{8}$$

where $\psi(f,\phi)$ and R are the phase pattern of the antenna element and the distance between the probe antenna and the phase center of the measured antenna, respectively. Since the phase patterns of these three antennas are quite stable over 28-30 GHz as discussed before, the phase difference between adjacent frequency points at any observed angle in the azimuth plane can be described as

$$\triangle\Phi_n = -\frac{2\pi(f_{n+1} - f_n)R}{c}, \tag{9}$$

where f_n is the n-th frequency point, $n \in [1, 1000]$. To eliminate the measurement uncertainties, $\triangle\Phi_n$ is divided into M groups and we get average value u_m for each group.

Then, the estimated R for different frequency groups can be calculated using (9) as

$$R_m = -\frac{u_m \cdot c}{2\pi\Delta f}, \tag{10}$$

where Δf is the frequency interval between two adjacent frequency points and M is chosen as 10 in our case. The standard deviation of R_m has been implemented to evaluate the shift level, i.e., stability of the phase center, which is defined as

$$\sigma = \sqrt{\frac{1}{M}\sum_{m=1}^{m=M}(R_m - \overline{R_m})^2}, \tag{11}$$

where $\overline{R_m}$ is the average of R_m. When σ is much smaller than the aperture dimension of the virtual array, the phase center of this antenna element could be considered stable. In our measurements, the σ of biconical antenna is less than 0.91 cm for all the observation angle in the azimuth plane. The σ of corrugated and horn antennas are 1.93 cm and 2.33 cm within the observation angle range of [-90°, 90°] and [-140°, 140°], respectively. Although the σ of the directional antenna is bigger than the omni-directional antenna, it is still much smaller than the diameter of the UCA discussed in this paper.

To summarize, phase patterns of these two directional antennas in each direction are approximately unchanged over frequencies within the main beam width. Although the phase patterns of directional antennas vary in a large angular range, the phase patterns within the main beam range are approximately constant. Besides, the phase centers of these three antennas can be considered stable compared with the dimensions of virtual arrays. These characteristics provide possibilities of neglecting the compensation of phase pattern for directional antenna based VAA. These are preconditions for the proposed method discussed later.

C. Modified Classical Beam-forming Algorithm

Based on the phase pattern and phase center analysis in Section II-B, we attempt to propose a practical and simple modified classical beamformer for directional antenna based UCA without considering the antenna phase pattern. As discussed, this is desired for practical measurements, since element phase pattern is typically not available or difficult to measure accurately. The following simulations are based on a far-field assumption and the measured complex radiation pattern in Section II-B are used to calculate the beamforming results.

The simplest way to achieve beamforming for directional antenna based UCA is to apply the same array weights as omnidirectional antenna based UCA in (7) i.e., using CBF algorithm. The normalized array beam pattern of biconical, corrugated and horn antennas using CBF are shown in black line in Fig. 4 (a), and black dotted line in 4 (b), 4 (c), respectively. The biconical antenna based UCA is used for comparison. The analysis of simulation and measurement results of biconical antenna based VAA in the rest of the paper will all apply array weights in (7). A high back-lobe appears in the array beam pattern of the directional antenna

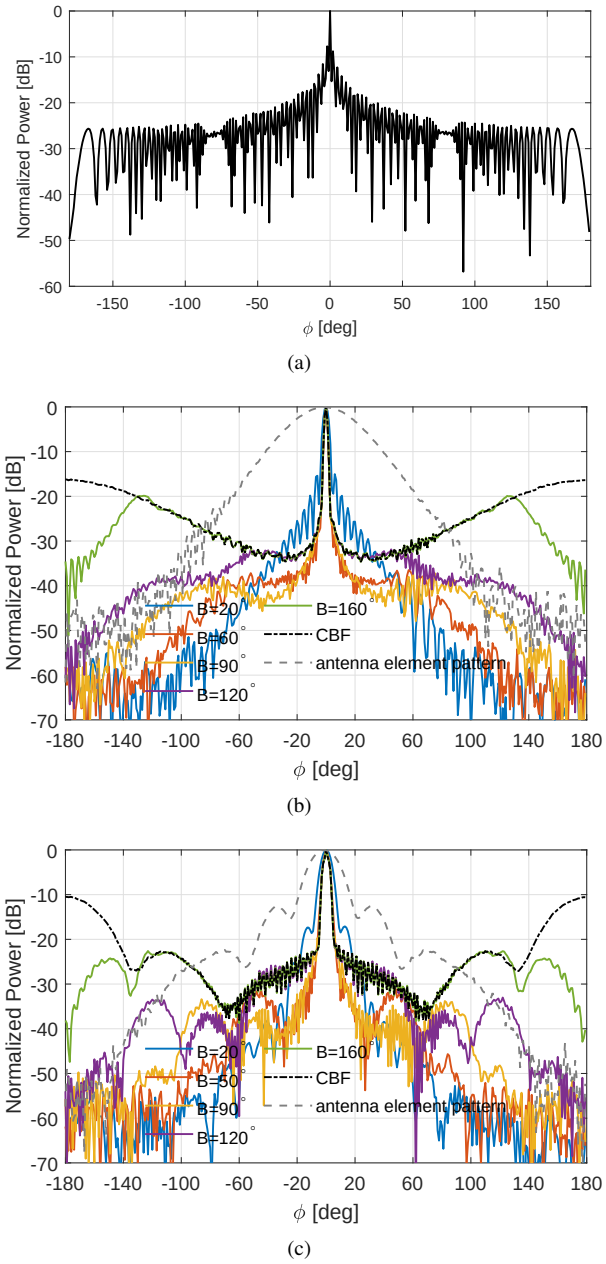

Fig. 4. (a) The array beam pattern of biconical antenna based UCA using CBF algorithm. The antenna element and array beam pattern of (b) corrugated antenna based UCA, and (c) horn antenna based UCA.

based UCA whereas the biconical based UCA provides high angular resolution without back lobe. The main reason for the back-lobe is that the array elements have very different antenna gain given a certain observation angle in the azimuth plane for directional antenna based UCA as depicted in Fig. 1, whereas array elements have equal gain for the omnidirectional antenna based UCA. Assuming the directivity of the UCA is the highest at $\phi = \phi_0$, the phase of the directional array elments located towards the direction of ϕ_0 can be partly aligned when calculating the array beam pattern at $\phi = \phi_0 + 180°$ resulting in the high back-lobe. Therefore, the array weighting method adopted for conventional VAA scheme cannot be applied directly, and there is a need for a new array weighting

method. To address this problem, a window function filtered array weighting strategy is proposed as

$$\omega_p = \exp[-\frac{j2\pi fr}{c} cos(\phi - \varphi_p)] \cdot s(\phi), \tag{12}$$

where $s(\phi)$ is the window function which is define by

$$s(\phi) = \begin{cases} 0, \mid \phi - \varphi_p \mid > B \\ 1, \mid \phi - \varphi_p \mid \leqslant B, \end{cases} \tag{13}$$

where B is the selected angle range and the phase of $(\phi - \varphi_p)$ is wrapped within $(-180°, 180°)$.

Since the phase pattern is flat and phase center is relatively stable in the main beam for directional antennas, phase pattern compensation is not considered in (11). The basic idea is to include only effective antenna elements according to the observation angle ϕ and remove the undesired interference from other array elements in the beamforming procedure. The window function is used to select only the array elements which locate inside a certain range to achieve beamforming given an observation angle in azimuth plane, as shown in the shadow parts in Fig. 1. The array elements included in the beamforming procedure will adapt according to the observation angle ϕ varies (see different shadow parts with $\phi = -90°$ or 180°, shown in Fig. 1).

The array beam patterns with different value of B are given in Fig. 4 (b) (c) for corrugated and horn antenna based UCA, respectively. When B is set as a small value, e.g., 20°, not enough effective elements are included in the UCA, resulting in insufficient angular resolution and sidelobe suppression as seen the blue curves in Fig. 4 (b) and (c). On the other hand, the back lobe becomes obvious when B is larger than 120°. Compared with the single antenna pattern, significant improvements on angular resolution can be obtained when B is within the range of [60°, 90°] and [50°, 90°] for corrugated antenna and horn antenna, respectively. Moreover, the sidelobe level is around -40 dB and -33 dB for corrugated antenna and horn antenna, respectively, whereas the sidelobe level in Fig. 4 (a) is around -25 dB. It can be observed that the proposed beamformer is efficient for directional antenna based UCA to improve the angular resolution and suppress side lobes compared with single directional antenna and conventional omnidiretional antenna based UCA, respectively.

When the complex antenna pattern is available, it is straightforward to achieve the best choice of the window width by simulating the array beam pattern using different value of B. However, a 90° window can be a conservative choice to include enough effective array elements and control the back lobe power for different types of directional antennas when the complex antenna pattern is not at hand. Note that a smaller value of B might be enough for more directive antennas. The angular resolution for a UCA in our discussion is mainly determined by the antenna element pattern, i.e., the beam-width of the main lobe, and the array size, i.e. the radius of the UCA. In practical, with the virtual array concept, the angular resolution will not be a problem since the number of virtual array elements and array size can be set sufficiently large, while the side-lobe effects and the SNR are more important. When the element pattern, window width and the size of UCA remain the same, only array gain will be improved as the number of array elements becomes bigger. However, no obvious differences can be observed in terms of angular resolution and side lobe level since the effective array aperture does not change. Therefore, similar parameter estimation performances can be achieved as long as the number of the array elements in the UCA fulfills the requirement of avoiding spatial aliasing given a fixed size of UCA and window width. Note that the array element number P is set as 360 in all our measurements since the measurements are fully automated and the measurement time is acceptable.

TABLE III
PATH PARAMETERS

Path index	1	2	3
α [dB]	0	-3	-9
ϕ [deg]	-60	0	-60
τ [ns]	20	60	60

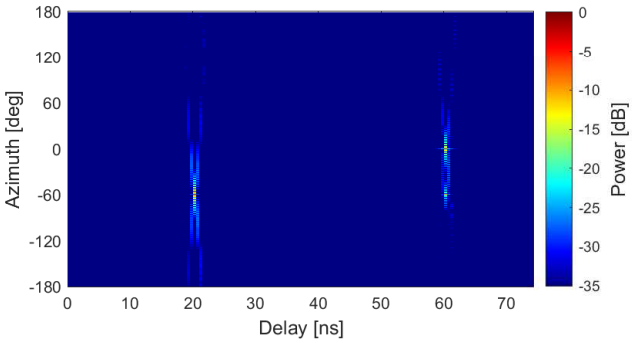

Fig. 5. PADP of biconical antenna based VAA.

III. SIMULATION RESULTS AND DISCUSSIONS

In this section, the comparisons of the simulation results between DSS method, conventional omni-directional antenna based VAA, and the proposed directional antenna based VAA are provided and discussed. The conventional VAA and the directional antenna based VAA use the classical and modified classical (i.e., with window function) beamforming algorithms, respectively, to achieve the beamforming results and then obtain the PADP, whereas the PADP of DSS method is directly calculated from the measured frequency response at each pointing angle. In the simulation, a UCA composed of 360 antenna elements with radius 0.2 m is considered. The measured complex radiation patterns are also used in the simulation. The window width B is chosen as 90° for both the corrugated antenna and horn antenna based UCAs.The frequency band is from 28-30 GHz with 1001 frequency points. A representative scenario with three paths was simulated as summarized in Table III. The impinging angles, amplitude and delay of three paths are designed to demonstrate the proposed method in a critical scenario.

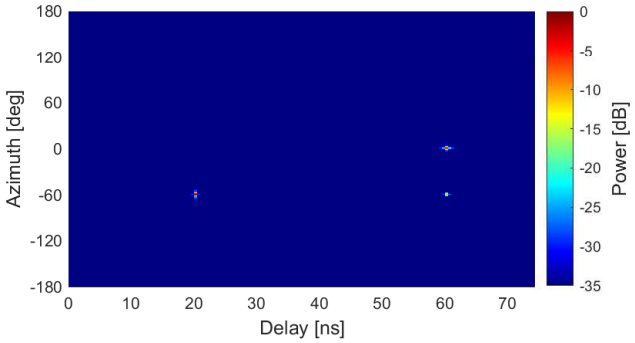

(a)

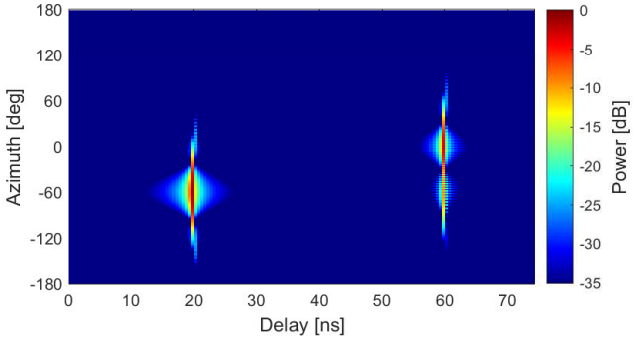

(b)

Fig. 6. PADPs based on (a) proposed method and (b) DSS method using corrugated antenna.

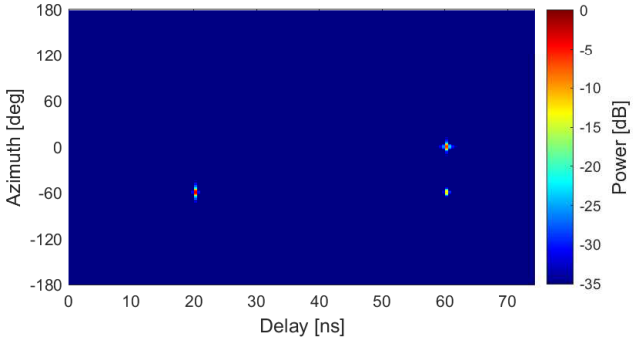

(a)

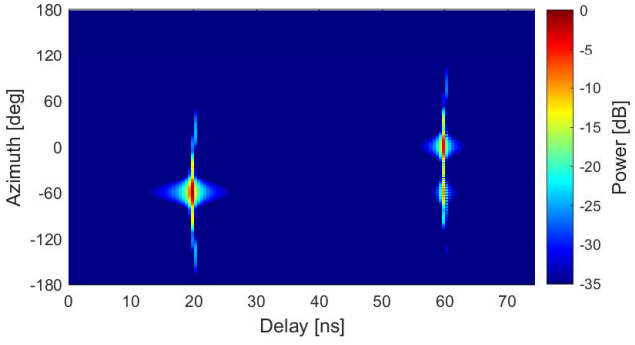

(b)

Fig. 7. PADPs based on (a) proposed method and (b) DSS method using horn antenna.

TABLE IV
THE ESTIMATED AMPLITUDE OF MPCS

Antenna type	Path 1	Path 2	Path 3
Biconical antenna	-1.0 dB	-4.2 dB	-10.2 dB
Corrugated antenna	-0.8 dB	-4.0 dB	-10.0 dB
Horn antenna	-2.5 dB	-5.6 dB	-11.4 dB

The power angle delay profiles (PADPs) using biconical, corrugated and horn antennas are given in Fig. 5, Fig. 6. and Fig. 7, respectively. Note that the antenna gains are removed with the knowledge of the amplitude of antenna patterns. In Fig. 5, the PADP of biconical antenna based VAA, though with high angular resolution, suffers from high joint sidelobes in both delay and angle domains, which was detailed in [34]. Path 2 and path 3 are difficult to be separated using DSS method as shown in Fig. 6 (b) and Fig. 7 (b). The proposed method greatly improves the angular resolution and efficiently suppresses the side lobe effects as shown in Fig. 6 (a) and Fig. 7 (a). Comparing the results of corrugated antenna and horn antenna, corrugated antenna has a better angular resolution. The estimated angle of arrivals (AOAs) and delay of both biconical antenna and directional antenna based VAA schemes achieve excellent consistency with the pre-set values. The estimated path amplitude using different methods are concluded in Table IV. The biconical, corrugated and horn antenna based VAAs have the maximum 1.2 dB, 1 dB, 2.6 dB errors in path amplitude estimation. The errors of biconical antenna based VAA come from the non-ideal omnidirectional pattern as depicted in Fig. 2 (a). The power estimation errors of directional antenna based VAA are mainly caused by the uncompensated phase pattern, which makes the estimation power lower than the real value. Horn antenna has larger errors than corrugated antenna since it has a phase pattern with more violent fluctuation in the main beam. However, all the three methods can obtain quite accurate relative power estimation of MPCs.

Some requirements of the directional antennas used to form a VAA can be concluded from the previous analysis and the simulation results.

- A stable phase center which can be evaluated using (11). This guarantees that the configuration of the VAA is stable, i.e. the radius r of a UCA.
- A flat phase pattern in the main beam. In particular, at least the phase pattern deviation within the HPBW should be within [-10°, 10°] to ensure that the signals received by the array elements within the range of HPBW could be added up in phase in the beam-forming procedure. This is the prerequisite of the proposed modified CBF method and the requirement is more demanding when accurate power estimation of MPCs is expected.
- Appropriate beam-width of the main lobe. Wider beam-width can provide higher angular resolution given a fixed size UCA, however, lower antenna element gain in general, which indicates a smaller dynamic range in the measurements. An elaborate selection of the beam-width of the antenna element might be helpful to balance

the angular resolution and the dynamic range during the measurements. However, our measurement results have shown that the proposed scheme works well for the popular standard gain horn antenna and the corrugated antenna.

IV. Measurement Validations

To verify the proposed directional antenna based VAA system in practice, measurements were conducted in two static environments, i.e., an anechoic chamber and an indoor meeting room. Biconical antenna based VAA was measured and analyzed as a reference VAA scheme. For directional antennas, there are two groups of measurements. The first is to measure the channels using DSS method by setting the directional antenna at the rotation center and recording the data at each uniform angle in azimuth plane. This group of measurements are used as reference DSS measurements. The second group of measurements are used to validate the directional antenna based VAA framework. The UCA was realized virtually by mounting antenna element on a positional rotator. We obtained P = 360 elements of the UCA array by automatically positioning the antenna at uniform angles and the radius r (the distance between the antenna and the rotation center was 0.2 m for measurements in an anechoic chamber and 0.1 m in an indoor meeting room, respectively. Note that the measurement systems of the first and the second group are essentially the same except the position of the antenna relative to the rotation center. The frequency band is from 28 to 30 GHz with 1001 frequency samples for each uniform angle. It can be calculated that the delay resolution is 0.5 ns and the maximum measurement range is around 105 m given the bandwidth of 2 GHz. The transmit power for the indoor measurements is -5 dBm. For simplicity, the measurements with only one polarization are conducted for directional antenna based VAA. However, it is straightforward to conduct dual polarization measurements using the proposed method. In the following analysis, a dynamic range of 30 dB is considered for all plots.

A. Anechoic chamber measurements

We first validate the proposed method in an anechoic chamber with only one direct path radiated from the probe antenna as shown in Fig. 8. The probe antenna was fixed and the antenna used to form VAA was set on the rotator and the center of the antennas are aligned by laser with the same height as the probe antenna. The signals were excited by VNA and transmitted to probe antenna through cables, and the antenna used to form a VAA received signals and transmitted the signals back to VNA. $S_{21}(f)$ was measured to characterize the channels and the system response introduced by the cables could be removed via calibration.

The PADP measured with biconical antenna based VAA is shown in Fig 9. Fig. 10 depicts the PADPs based on VAA and DSS methods using corrugated antenna, while Fig. 11 for the horn antenna. Although the path can be identified in Fig. 9, the joint side lobes are obvious. In Fig. 10 (a) and Fig. 11 (a), the proposed method provides high angular

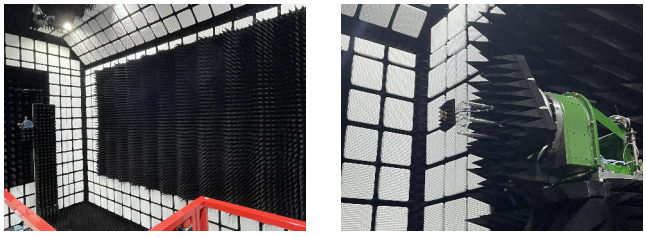

(a) (b)

Fig. 8. (a) The photo of the probe antenna. (b) The horn antenna used to form the VAA.

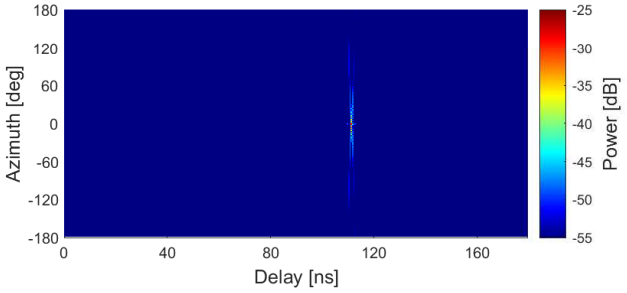

Fig. 9. PADP measured with biconical antenna based VAA in an anechoic chamber.

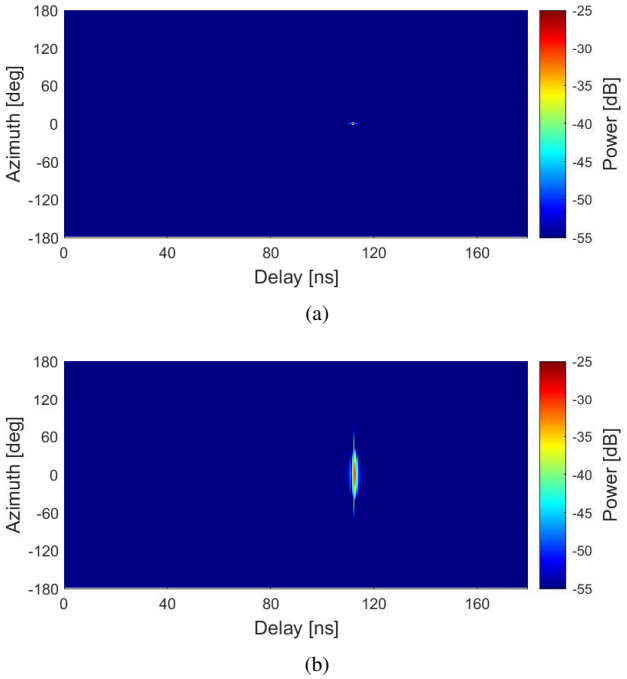

(a)

(b)

Fig. 10. PADPs based on (a) proposed method and (b) DSS method using corrugated antenna measured in an anechoic chamber.

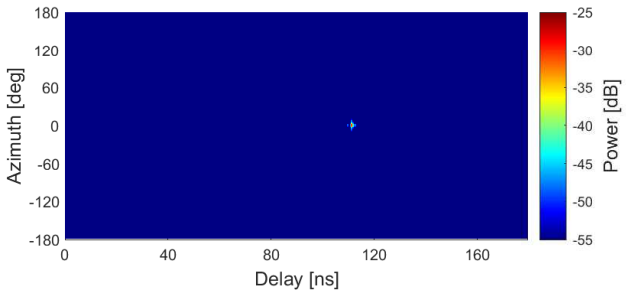

(a)

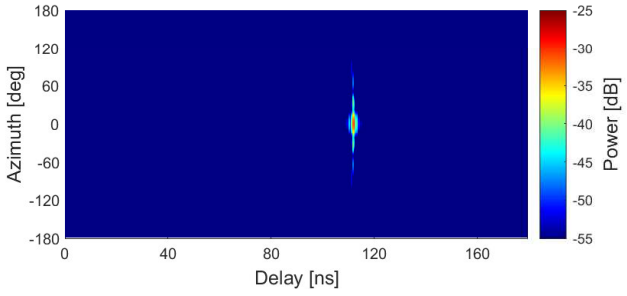

(b)

Fig. 11. PADPs based on (a) proposed method and (b) DSS method using horn antenna measured in an anechoic chamber

resolution in accordance with the simulation results. The horn antenna has high sidelobes, which may be identified as fake paths using DSS method as shown in Fig. 11 (b). The HPBW of the corrugated antenna is around 40°, resulting in a low angular resolution using DSS method as shown in Fig. 10 (b). However, the corrugated antenna provides a higher angular resolution than horn antenna using VAA scheme. The delay of the path can be accurately estimated by all methods. The path amplitude estimated by DSS method using horn antenna is -29.7 dB, which is used as a reference. The biconical, corrugated and horn antenna based VAA have 1.6 dB, 1.3 dB and 2.2 dB differences compared with the reference. Consistent results as in the simulation can be observed, i.e. best results acheived by the corrugated antenna, and worst results by the horn antenna.

B. Indoor measurements

The indoor measurements were conducted in a meeting room with some furniture and a metal plate with the dimensions of 56 mm × 85 mm which was placed between the antennas to form an obstructed line-of-sight (O-LOS) scenario, as shown in Fig. 12. The O-LOS scenario includes rich MPCs with a few dominant paths from different directions. The measurement system consists of a VNA, two cables, Tx, Rx antennas and a rotation platform. Transceiver (Tx) antenna is a corrugated antenna which operates over 24-38 GHz with a HPBW of 40°. The receiver (Rx) antenna specifications are listed in Table I. The transmission of the signal is similar to that in the anechoic chamber. However, we need to move the antenna from the rotation center to a position of 0.1 m away manually to form a VAA, which may introduce uncertainties

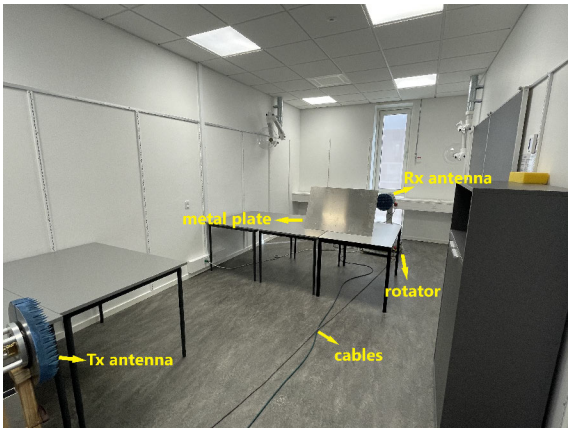

Fig. 12. The photo of the meeting room.

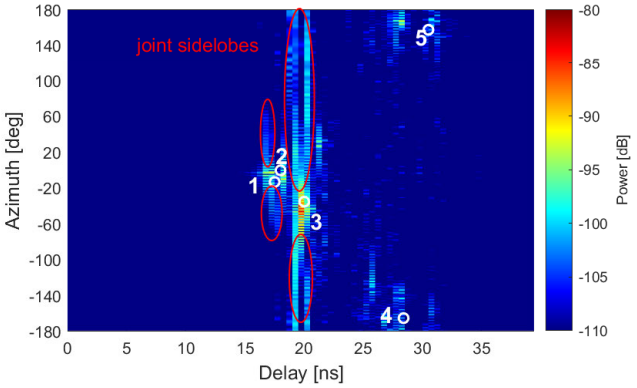

Fig. 13. PADP measured with biconical antenna based VAA in a meeting room.

in the radius of the UCA. Both Tx and Rx antennas were all placed 93 cm above the floor. The center of Tx and Rx antennas were aligned manually and required alignment every time when changing the Rx antenna, which may bring some non-stationarity to the channel profiles. The back-to-back calibration was conducted before measuring the channels.

Fig. 13, Fig. 14 (a), and Fig. 15 (a) show the PADPs of biconical, corrugated, and horn antenna based VAAs, respectively. The differences between the PADPs measured by biconical, corrugated and horn antennas based VAAs as shown in Fig. 13, Fig. 14 (a), and Fig. 15 (a), are mainly caused by the following two reasons. Firstly, the side-lobe effects of the omni-directional antenna based VAA are severe using CBF algorithm. The CBF is achieved by shifting the phase of each element frequency response into alignment, the frequency-dependent phase shift also generates side-lobes which vary according to the frequency of operation [34]. As a result, the joint side-lobes in delay and angle domains (seen in Fig. 13) can be identified as fake paths in channel characterization. However, the joint side-lobes are not observed in PADP measured with directional antenna based VAA since the side-lobes are very weak. Besides, the HPBW of biconical, corrugated and horn antennas in the vertical plane is different. Although we only consider a 2-D angular domain in our estimation, the Rx antennas can receive the paths coming from a 3D scenario

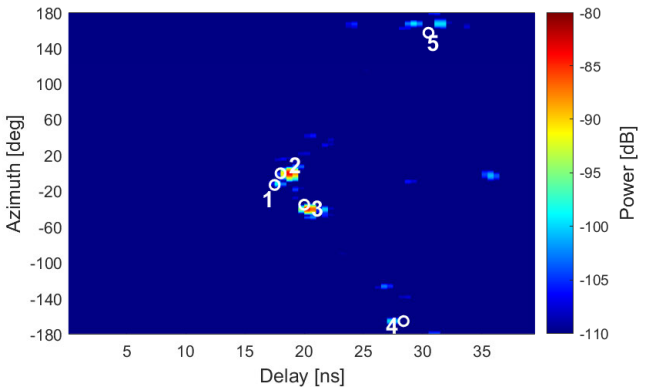

(a)

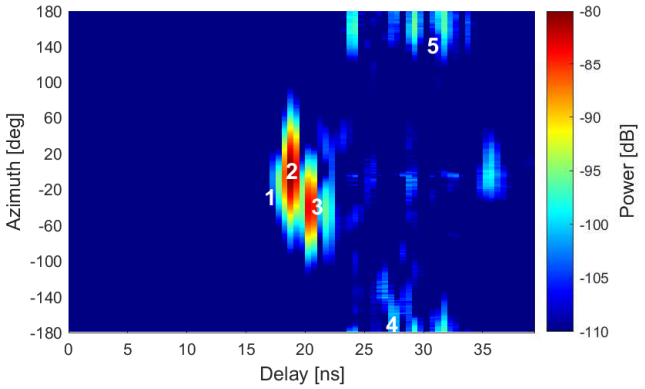

(b)

Fig. 14. PADPs based on (a) proposed method and (b) DSS method using corrugated antenna measured in a meeting room.

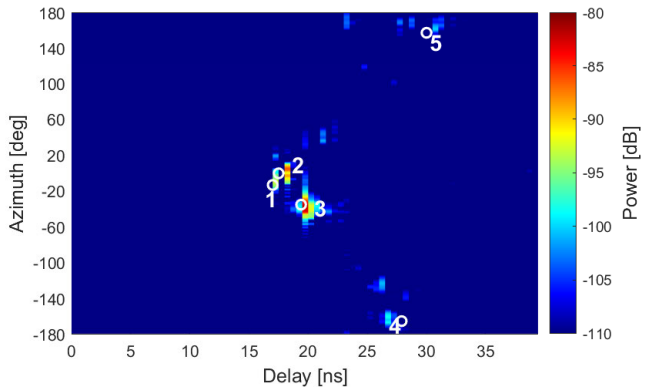

(a)

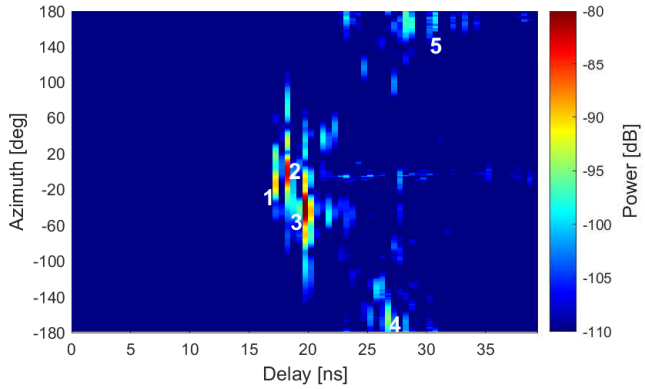

(b)

Fig. 15. PADPs based on (a) proposed method and (b) DSS method using horn antenna measured in a meeting room.

TABLE V
PATH PARAMETERS OF THE INDOOR MEASUREMENTS

Path no.	Corrugated antenna based VAA		Ray-tracer	
	AoA (deg)	delay (ns)	AoA (deg)	delay (ns)
1	-12	17	-13	17.2
2	0	18	0	17.5
3	-39	19.5	-35	19.4
4	-165	27	-165	27.9
5	168	30.5	158	30.0

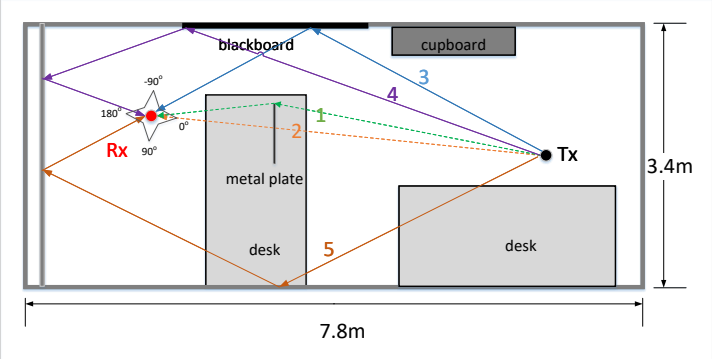

Fig. 16. Trajectory of the MPCs in relation to the room geometry. The dashed lines represents the diffraction paths.

in practice. Therefore, antennas with wider HPBW in vertical planes might capture more paths than antennas with narrower HPBW. The PADP measured by directional antennas using DSS method are shown in Fig. 14 (b) and Fig. 15 (b). They are used as references to discuss about the estimation accuracy of angle of arrival (AOA) and delay of MPCs. The five dominant paths are marked in all PADPs.

Path 1 and path 2 are the diffraction paths passing over the top and right edge of the metal plate, respectively. Path 3 is the reflection wave from the cupboard. Path 4 is the second order reflection on the blackboard and wall whereas path 5 is the second order reflection on the left wall and the back wall. The path trajectories of the channel measurements in the meeting room are shown in Fig. 16. For simplicity, we assume only low-order bounces, i.e., (up to 2 bounces) for specular reflection and one bounce for diffraction in our ray tracer. We have marked the paths obtained from the ray tracer with white circles on the PADPs measured by VAA schemes as shown in Fig. 13, Fig. 14 (a) and Fig. 15 (a). The five dominant paths can be identified and the estimated delay of MPCs are in accordance with the references for all directional antenna based VAA schemes. The AOA of path 1 and path 2 shown in Fig. 13 has around 8° difference from the results of DSS method shown in Fig. 15 (b) whereas the other three paths are matched well. The metal plate has to be removed when doing the alignment of antenna center for each measurement. The positioning error of the mental plate might cause the

change of the AOA of path 1 and path 2. Since the estimated parameters of the dominant paths obtained from corrugated antenna and horn antenna based VAAs have good agreement with each other, we only compare the results obtained from the corrugated antenna based VAA and ray tracer as shown in Table V. The parameters obtained from the measurements agree well with the ray tracing results. Small differences might come from the measurement errors of the dimensions and locations of the obstacles. Comparing the estimated DOA and AOA using proposed method with those using DSS method, a good match can be observed for both corrugated antenna and horn antenna. Besides, the corrugated antenna based VAA provides higher angular resolution than the horn antenna based VAA. The sidelobes of horn antenna in Fig. 15 (a) is efficiently suppressed using the proposed method in comparison with the DSS method.

V. Conclusion

In this paper, we propose a novel directional antenna based VAA framework and window function filtered weighting method to characterize the mm-Wave band channels. The phase pattern and phase center stability of two representative directional antennas, i.e, a horn antenna and a corrugated antenna are analyzed. The angular resolution and SNR are significantly improved, and the side lobes are efficiently suppressed in PADP results with the proposed method, as validated in the simulations and experiments. Directional antenna based VAA shows advantages over DSS and omnidirectional antenna based VAA. Besides, the comparison of two different directional antenna based VAAs provides instructions of selecting the directional antenna element forming a VAA. The proposed directional antenna based VAA framework has promising applications in achieving accurate channel characterization in both vertical and horizontal polarizations for mm-Wave and sub-THz bands, which might break through the current bottleneck in channel characterization.

In addition, the proposed method still has chances to further improve the SNR and suppress the side lobes. Moreover, the proposed concept has promising applications in sub-THz channel modeling and estimation. These possible extensions will be considered in our future works.

Acknowledgment

The authors would like to thank for the assistance offered by Yejian Lv, Zhiqiang Yuan and Kim Olesen during the measurement campaigns.

References

[1] T. S. Rappaport, S. Sun, R. Mayzus, H. Zhao, Y. Azar, K. Wang, G. N. Wong, J. K. Schulz, M. Samimi, and F. Gutierrez, "Millimeter wave mobile communications for 5g cellular: It will work!" *IEEE Access*, vol. 1, pp. 335–349, 2013.

[2] K. Guan, G. Li, T. Kürner, A. F. Molisch, B. Peng, R. He, B. Hui, J. Kim, and Z. Zhong, "On millimeter wave and thz mobile radio channel for smart rail mobility," *IEEE Trans. Veh. Technol.*, vol. 66, no. 7, pp. 5658–5674, 2016.

[3] R. He, B. Ai, G. L. Stüber, G. Wang, and Z. Zhong, "Geometrical-based modeling for millimeter-wave mimo mobile-to-mobile channels," *IEEE Trans. Veh. Technol.*, vol. 67, no. 4, pp. 2848–2863, 2017.

[4] D. Dupleich, R. Müller, S. Skoblikov, M. Landmann, G. Del Galdo, and R. Thomä, "Characterization of the propagation channel in conference room scenario at 190 ghz," in *2020 14th European Conference on Antennas and Propagation (EuCAP)*. IEEE, 2020, pp. 1–5.

[5] C. Gustafson, K. Haneda, S. Wyne, and F. Tufvesson, "On mm-wave multipath clustering and channel modeling," *IEEE Trans. Antennas Propag.*, vol. 62, no. 3, pp. 1445–1455, 2013.

[6] R. He, B. Ai, A. F. Molisch, G. L. Stuber, Q. Li, Z. Zhong, and J. Yu, "Clustering enabled wireless channel modeling using big data algorithms," *IEEE Commun. Mag.*, vol. 56, no. 5, pp. 177–183, 2018.

[7] S. Hur, S. Baek, B. Kim, Y. Chang, A. F. Molisch, T. S. Rappaport, K. Haneda, and J. Park, "Proposal on millimeter-wave channel modeling for 5g cellular system," *IEEE J. Sel. Topics Signal Process.*, vol. 10, no. 3, pp. 454–469, 2016.

[8] X. Zhao, F. Du, S. Geng, Z. Fu, Z. Wang, Y. Zhang, Z. Zhou, L. Zhang, and L. Yang, "Playback of 5g and beyond measured mimo channels by an ann-based modeling and simulation framework," *IEEE journal on selected areas in communications*, vol. 38, no. 9, pp. 1945–1954, 2020.

[9] L. Tian, V. Degli-Esposti, E. M. Vitucci, and X. Yin, "Semi-deterministic radio channel modeling based on graph theory and ray-tracing," *IEEE Trans. Antennas Propag.*, vol. 64, no. 6, pp. 2475–2486, 2016.

[10] E. Vitucci, J. Chen, V. Degli-Esposti, J. Lu, H. Bertoni, and X. Yin, "Analyzing radio scattering caused by various building elements using millimeter-wave scale model measurements and ray tracing," *IEEE Trans. Antennas Propag.*, vol. 67, no. 1, pp. 665–669, 2018.

[11] T. S. Rappaport, G. R. MacCartney, M. K. Samimi, and S. Sun, "Wideband millimeter-wave propagation measurements and channel models for future wireless communication system design," *IEEE Trans. Commun.*, vol. 63, no. 9, pp. 3029–3056, 2015.

[12] C. Ling, X. Yin, R. Müller, S. Häfner, D. Dupleich, C. Schneider, J. Luo, H. Yan, and R. Thomä, "Double-directional dual-polarimetric cluster-based characterization of 70–77 ghz indoor channels," *IEEE Trans. Antennas Propag.*, vol. 66, no. 2, pp. 857–870, 2017.

[13] G. R. Maccartney, T. S. Rappaport, S. Sun, and S. Deng, "Indoor office wideband millimeter-wave propagation measurements and channel models at 28 and 73 ghz for ultra-dense 5g wireless networks," *IEEE Access*, vol. 3, pp. 2388–2424, 2015.

[14] S. Salous, V. Degli Esposti, F. Fuschini, R. S. Thomae, R. Mueller, D. Dupleich, K. Haneda, J.-M. M. Garcia-Pardo, J. P. Garcia, D. P. Gaillot *et al.*, "Millimeter-wave propagation: Characterization and modeling toward fifth-generation systems.[wireless corner]," *IEEE Antennas Propag. Mag.*, vol. 58, no. 6, pp. 115–127, 2016.

[15] C. U. Bas, R. Wang, S. Sangodoyin, D. Psychoudakis, T. Henige, R. Monroe, J. Park, C. J. Zhang, and A. F. Molisch, "Real-time millimeter-wave mimo channel sounder for dynamic directional measurements," *IEEE Trans. Veh. Technol.*, vol. 68, no. 9, pp. 8775–8789, 2019.

[16] D. Caudill, P. B. Papazian, C. Gentile, J. Chuang, and N. Golmie, "Omnidirectional channel sounder with phased-arrayantennas for 5g mobile communications," *IEEE Transactions on Microwave Theory and Techniques*, vol. 67, no. 7, pp. 2936–2945, 2019.

[17] C. U. Bas, R. Wang, S. Sangodoyin, T. Choi, S. Hur, K. Whang, J. Park, C. J. Zhang, and A. F. Molisch, "Outdoor to indoor propagation channel measurements at 28 ghz," *IEEE Transactions on Wireless Communications*, vol. 18, no. 3, pp. 1477–1489, 2019.

[18] H. Tataria, E. L. Bengtsson, O. Edfors, and F. Tufvesson, "27.5-29.5 ghz switched array sounder for dynamic channel characterization: Design, implementation and measurements," *arXiv preprint arXiv:2105.10712*, 2021.

[19] R. Wang, O. Renaudin, C. U. Bas, S. Sangodoyin, and A. F. Molisch, "On channel sounding with switched arrays in fast time-varying channels," *IEEE Trans. Wireless Commun.*, vol. 18, no. 8, pp. 3843–3855, 2019.

[20] J. O. Nielsen, W. Fan, P. C. Eggers, and G. F. Pedersen, "A channel sounder for massive mimo and mmwave channels," *IEEE Commun. Mag.*, vol. 56, no. 12, pp. 67–73, 2018.

[21] A. F. Molisch, *Wireless communications*. John Wiley & Sons, 2012, vol. 34.

[22] W. Fan, I. Carton, J. Ø. Nielsen, K. Olesen, and G. F. Pedersen, "Measured wideband characteristics of indoor channels at centimetric and millimetric bands," *EURASIP Journal on Wireless Communications and Networking*, vol. 2016, no. 1, pp. 1–13, 2016.

[23] G. Zhang, K. Saito, W. Fan, X. Cai, P. Hanpinitsak, J.-I. Takada, and G. F. Pedersen, "Experimental characterization of millimeter-wave indoor propagation channels at 28 ghz," *IEEE Access*, vol. 6, pp. 76 516–76 526, 2018.

[24] A. W. Mbugua, W. Fan, Y. Ji, and G. F. Pedersen, "Millimeter wave multi-user performance evaluation based on measured channels with virtual antenna array channel sounder," *IEEE Access*, vol. 6, pp. 12 318–12 326, 2018.
[25] S. Ranvier, J. Kivinen, and P. Vainikainen, "Millimeter-wave mimo radio channel sounder," *IEEE transactions on Instrumentation and Measurement*, vol. 56, no. 3, pp. 1018–1024, 2007.
[26] K. Fan, Z.-C. Hao, Q. Yuan, J. Hu, G. Q. Luo, and W. Hong, "Wideband horizontally polarized omnidirectional antenna with a conical beam for millimeter-wave applications," *IEEE Trans. Antennas Propag.*, vol. 66, no. 9, pp. 4437–4448, 2018.
[27] 3GPP, "Study on radiated metrics and test methodology for the verification of multi-antenna reception performance of nr user equipment (ue)," 2021, tR 38.827., Oct. 2021. [Online]. Available: https://www.3gpp.org
[28] A. Karttunen, J. Järveläinen, S. L. H. Nguyen, and K. Haneda, "Modeling the multipath cross-polarization ratio for 5–80-ghz radio links," *IEEE Trans. Wireless Commun.*, vol. 18, no. 10, pp. 4768–4778, 2019.
[29] H. Krim and M. Viberg, "Two decades of array signal processing research: the parametric approach," *IEEE Signal Process. Mag.*, vol. 13, no. 4, pp. 67–94, 1996.
[30] P. Stoica, R. L. Moses *et al.*, "Spectral analysis of signals," 2005.
[31] A. Systems, "Data sheet for sas-574." 2021, accessed 4 March 2021. [Online]. Available: https://www.ahsystems.com/catalog/SAS-574.php
[32] A. S. S. (ASYSOL), "Data sheet for asy-cwg-s-265." 2021, accessed 4 March 2021. [Online]. Available: https://asysol.com/portfolio/circular-corrugated-feeds/
[33] A-INFO, "Data sheet for biconical antenna sz-2003000/p." 2021, accessed 4 March 2021. [Online]. Available: https://www.ainfoinc.com/antenna-products/bi-conical-antennas/sz-2003000-p-bi-conical-antenna-2-30-ghz-0db-gain-sma-female
[34] C. Gentile, A. J. Braga, and A. Kik, "A comprehensive evaluation of joint range and angle estimation in ultra-wideband location systems for indoors," in *2008 IEEE International Conference on Communications*. IEEE, 2008, pp. 4219–4225.